

Blazar Boosted ALP and vector portal Dark matter confronting light mediator searches

Sk Jeusun^{1,*}

¹*School of Physical Sciences, Indian Association for the Cultivation of Science,
2A & 2B Raja S.C. Mullick Road, Kolkata 700032, India*

Abstract

The trouble in detecting low mass dark matter due to its low kinetic energy can be ameliorated in the boosted dark matter framework, where a sub-population of galactic dark matter attains very high energy after being up-scattered by energetic standard model particles. However, in such a scenario the upper limits on the cross-section obtained hitherto are typically large. Hence in the minimal extension of standard model where new mediators act as a portal between the dark and visible sectors, the direct detection limits for sub-GeV dark matter might lie within the exclusion region of other ground based searches of the mediator. To evade this deadlock, we allude to blazar boosted dark matter electron scattering in multi-ton neutrino detector Super kamiokande. We consider minimal models such as axion like particle (ALP) and vector portal dark matter being upscattered by high energy blazar jet and analyse the interesting parameter reaches from Super kamiokande in the parameter space of the mediator, surpassing the existing constraints. Besides, this scenario exhibits stronger limits for previously unexplored ALP mediated sub-MeV dark matter search which is difficult due to associated momentum suppression.

I. INTRODUCTION

Numerous astrophysical and cosmological observations have evinced the presence of a non luminous non baryonic component satisfying 25% of the total energy budget of the universe coined as dark matter (DM) [1–4]. The particle nature of DM persists to be an enigma for standard model (SM) of particle physics with its present set up despite the observational evidence [5–7]. To resolve this intriguing puzzle, the SM particle content is often augmented to include one or more beyond standard model (BSM) particles [7, 8]. The possibility of the existence of non-zero interactions between DM and SM particles other than the gravitational one, has framed the pathway of detecting it in the direct detection experiments [7, 9, 10]. Direct detection experiments like XENONnT [11, 12], LUX-ZEPLIN (LZ) [13, 14], Panda X-II [15], LUX [16], DEAP-360 [17], DarkSide-50 [18] try to explore possible interaction of an incoming DM with nucleon or electron in the ground based detectors while the solar system moves through the galactic DM halo [10].

All these experiments have placed strong constraints on $\mathcal{O}(\text{GeV})$ scale DM nucleon (electron) cross-sections, pushing the limits almost towards the neutrino floor [14]. Despite all the heroic efforts, no direct evidence of particle DM has motivated the community to search for low mass (sub-GeV) DM. However, current experiments face severe challenge to detect the low mass DM as its low velocity (10^{-3}) falls short of generating sufficient recoil energy above the threshold ($\sim \mathcal{O}(1)$ keV) of the ongoing detectors. To probe such light DM consideration of a sub-population of it exceeding the galactic escape velocity upon scattered by high energy cosmic ray [19, 20], diffuse supernova neutrinos [21, 22] has gained a lot of interests in last few years. In such boosted DM (BDM) sce-

nario the galactic DM particles after being up-scattered by the homogeneous high energetic particles, are expected to scatter again with the target particles in the earth based DM or neutrino detectors, null observations of which leads to constraint on the cross-section with nucleon (electron) [20, 23–25]. However, the probability of galactic DM being up-scattered by the cosmic particles and achieving high energy is very small and hence the constraints on the cross-section of sub GeV boosted DM is much smaller than those of galactic DM (with mass \gtrsim GeV) [20, 23]. Recently it has also been observed that the BDM flux and the constraints differ significantly depending on the Lorentz structures of the interaction between DM and nucleon (or, electron) [26–28]. Since the cross-sections probed by such boosted DM is typically large, it is crucial to consider minimal models of the sub-GeV DM-nucleon (electron) interaction and scrutinize whether the new regions probed by direct search are allowed by the other existing constraints on the model parameters. Novel studies in this have already investigated minimal models featuring a BSM mediator coupled to sub-GeV DM and nucleon [29] or electron [30], and pointed out that the direct detection constraints (for BDM) struggle to beat the existing constraints on the mediators coming from astrophysics and several ground based experiments.

An alternate avenue to boost light DM that has been explored recently, is the upscattering of DM by blazar jet [31, 32]. Blazar jet is the emitted jet of high energy particles from the active galactic nuclei (AGN) with a supermassive black hole (BH) at the center, in close alignment to the line of sight (LOS) from earth [33]. Being a luminous source the properties of blazars are delineated by the photon observations and are subject to modeling of the spectral energy distribution (SED) of the emitted photon [34]. Depending on the model blazars can emit highly energetic flux of electrons or protons. On the other hand the BH at the center can accumulate a huge amount of DM particles leading to a spike density signifi-

*Electronic address: skjeusun48@gmail.com

cantly larger than the galactic DM density [35]. Thus the relativistic jet can up-scatter the surrounding DM particles producing a significant amount of high energy (low mass) DM flux at earth [31, 32, 36, 37]. Since the blazar boosted DM (BBDM) has energy larger than the threshold energy of neutrino detectors like Super Kamiokande [38], the larger detector size and higher flux may provide stronger constraints on the DM SM cross-sections than other boosted DM scenarios [36, 37]. Though the models of blazar spectrum are subject to astrophysical uncertainty, exploring minimal BBDM models with light mediators can be a legitimate exercise to gain new insights into the particle aspects of low mass DM.

Motivated by this, in this work we study low mass DM boosted by blazar jet considering a fermion DM χ coupled to electrons (e) via a light mediator. As a case study we first look into the well motivated axion like particle (ALP) a as mediator. ALP is referred to signify a broad class of pseudo-Nambu Goldstone bosons (pNGB) associated with the spontaneously broken global symmetry [39]. ALP mediated DM has been explored widely for its rich phenomenological prospects [40, 41]. However, detection of ALP portal sub-GeV/MeV BDM is difficult due to momentum suppression of incoming DM, leading to poor direct detection constraints [29]. On the other hand experiments like BaBar [42], NA64 [43] place strong constraints on the ALP parameter space, making it a real challenge for the BDM detection scenario to probe any new parameter space. We explore such ALP portal DM boosted by the energetic blazar jet in the multi-ton neutrino detector Super Kamiokande (Super-K). Using the large fiducial volume and directional sensitivity Super-K has the ability to set the strongest limit on such BBDM scenario [32, 36]. As blazar source we consider the well studied TXS 0506+56 [44] and for comparison also showcase the effect of a less distant BL Lacertae [45]. Existence of TXS 0506+56 has been also indicated by the neutrino observations at IceCube [46], motivating the lepto-hadronic modeling of blazar jet [44]. Using the benchmark model parameters and state of the art formalism we first showcase the direct detection constraints on (sub) MeV scale ALP portal DM- e interaction and a significant portion of the obtained limits go beyond the bounds set by existing ALP search experiments. For a comparative analysis we also illustrate the constraints assuming a vector mediator. In the later part of this paper we carry out similar exercise with mediators that couple to both proton (p) and electron apart from DM, so that both of them potentially upscatter DM. As a consequence the incoming BBDM flux increases significantly due to the higher energetic flux of blazar protons, leading to stronger limits from Super-K.

We organize the paper as follows. In Sec.II we present the formalism of obtaining BBDM flux. Then we discuss the results for electrophilic DM in Sec.III and DM with both nucleon and electron coupling in Sec.IV. Finally we conclude in Sec.V. Some relevant calculations related to BBDM flux is shown in Appendix A.

II. BLAZAR BOOSTED DM FLUX

A. Flux of Blazar jet electrons:

The blazar jet is evaluated considering the popular “blob geometry” , assuming the particles are emitted isotropically from a homogeneous blob in the jet [31]. The blob moves with velocity β_B along the jet axis with respect to the rest frame of the BH center. For an observer in rest with respect to the BH, the corresponding Lorentz boost factor is given by, $\Gamma_B = \sqrt{1 - \beta_B^2}$. The angle of inclination of jet axis with respect to the line of sight (LOS) of observer is defined as θ_{LOS} .

For a given (lepto-)hadronic model the energy spectrum of the high-energetic particles in the blob frame is provided by a power law distribution [47],

$$\frac{d\Gamma'_i}{dE'_i d\Omega'} = \frac{1}{4\pi} c_i (E'_i/m_i)^{-\alpha_i}, \quad (1)$$

where E_i, m_i are the energy and mass of the emitted particle $i \in \{e, p\}$ respectively, and the “prime” in the superscript signifies the quantities to be in blob frame. c_i is the normalization constant computed from the predicted electron/proton luminosity L_i (shown in eq.(A7)). Quantities without a “prime” in the superscript refer them to be in observer’s rest frame. Here we focus on the electron jet ($i \equiv e$) which is predicted to be an essential component of blazar spectrum by several models of photon SED of blazars [47–49].

To obtain the boosted DM flux one needs the blazar jet spectrum of electrons in the observer’s frame given as (using eq.(A5))

$$\begin{aligned} \frac{d\Gamma_e}{dE_e d\Omega} &= \frac{1}{4\pi} c_e (E_e/m_e)^{-\alpha_e} \\ &\times \frac{\beta_j (1 - \beta_j \beta_B \mu)^{-\alpha_e} \Gamma_B^{-\alpha_e}}{\sqrt{(1 - \beta_j \beta_B \mu)^2 - (1 - \beta_j^2)(1 - \beta_B^2)}}, \end{aligned} \quad (2)$$

where, E' has been replaced by E using eq.(A2). We denote the kinetic energy (KE) of electron as $T_e = E_e - m_e$. $\mu = \cos \theta$, where θ is the angle with respect to jet axis in observer’s frame. $\beta_j, j = e$ is the speed of emitted particle given by, $\beta_j = \sqrt{1 - \gamma_e^{-2}}$, γ_e being E_e/m_e in rest frame. In blob frame E'/m_e has two cut-off in both high and low values i.e. γ'_{\max} and γ'_{\min} . For a particular SED $\gamma'_{\max}, \gamma'_{\min}, \alpha_e, L_e$ and the Doppler factor $\mathcal{D} = \Gamma_B^{-1} (1 - \cos \theta_{LOS})^{-1}$ are fitted to obtain these model parameters. For this work we consider the model parameters for TXS 0506+56 and BL Lacertae as pointed out in the existing literature [32]. Aforesaid five parameters along with θ_{LOS} , the mass of black hole (M_{BH}) in the AGN center and luminosity distance (d_L) are tabulated in table I. Throughout this paper in all the tables and figures we denote TXS 0506+56 (BL Lacertae) as “TXS” (“BLL”).

Parameter	TXS0506 + 56	BL Lacertae
$L_e(\text{erg/s})$	1.32×10^{44}	8.7×10^{42}
$(\gamma'_{\min}, \gamma'_{\max})$	$(500, 1.3 \times 10^4)$	$(700, 1.5 \times 10^4)$
\mathcal{D}	40	15
α_e	2.0	3.5
$\theta_{\text{LOS}}(^{\circ})$	0	3.82
$d_L(\text{Mpc})$	1835.4	322.7
$M_{\text{BH}}(M_{\odot})$	3.09×10^8	8.65×10^7

TABLE I: Model parameters for the blazar source TXS 0506+56 [44] and BL Lacertae [45].

B. DM density profile

If the super massive black hole (SMBH) at the centre of galaxy is grown adiabatically it is expected that a significant amount of DM particles would accumulate around it [35]. This type of enhanced DM density is referred as DM spike in the literature [50]. The DM density $\rho(r)$ follows a power law grading $\rho_1(r) \propto r^{-\gamma}$ within the spike radius R_{sp} [35]. Outside the spike DM density follows as usual NFW profile $\rho_2(r) \propto r^{-1}$. Generally the spike radius is taken to be $R_{sp} = 10^5 R_s$, where $R_s = 2GM_{\text{BH}}/c^2$ ($c = 1$ in natural unit) is the Schwarzschild radius [35, 50]. The DM density within the distance $4R_s$ from the galaxy center is expected to accrete and hence the density $\rho_1(r < 4R_s) = 0$. It is customary in literature to normalize the total DM mass within R_{sp} to be equal to M_{BH} , i.e. $\int_{4R_s}^{R_{sp}} d^3r \rho(r) = M_{\text{BH}}$. The normalization outside R_{sp} is obtained using the continuity at R_{sp} i.e. $\rho_2(R_{sp}) = \rho_1(R_{sp})$.

So far what we discussed is valid for non-annihilating DM. When DM particles annihilate, they may deplete the DM number density throughout the time scale. DM with number density n_{χ} and thermal averaged annihilation cross section $\langle \sigma v \rangle$ will reduce its density at a rate $\Gamma = n_{\chi} \langle \sigma v \rangle$. This will flatten the spike density and after time t_{BH} i.e. the age of black hole, the density will be [35],

$$\rho(r, t_{\text{BH}}) = \frac{\rho(r, t=0) \rho_{\text{core}}}{\rho(r, t=0) + \rho_{\text{core}}}, \quad (3)$$

where $\rho_{\text{core}} = m_{\chi} / \langle \sigma v \rangle t_{\text{BH}}$ is the maximum surviving density after t_{BH} , often known as saturation density in literature [35]. For non annihilating DM, $\langle \sigma v \rangle = 0$, $\rho(r, t_{\text{BH}}) = \rho(r, t=0)$.

In Fig.1(a) we show the variation of DM density with distance from BH center (in terms of R_s) with $\gamma = 7/3$ as used in literature [31, 32]. The solid and dotted line represents DM profile due to TXS 0506+56 and BL Lacertae respectively. The red, green and blue line correspond to the cases with $\langle \sigma v \rangle = 0, 10^{-28} \text{ cm}^3 \text{ s}^{-1}, 3 \times 10^{-26} \text{ cm}^3 \text{ s}^{-1}$. Note that the annihilation dilutes DM density and flattens the spike towards a core profile as expected from the discussion above. Following the same argument with an increase in $\langle \sigma v \rangle$ the density decreases. Another important quantity to determine the expected boosted

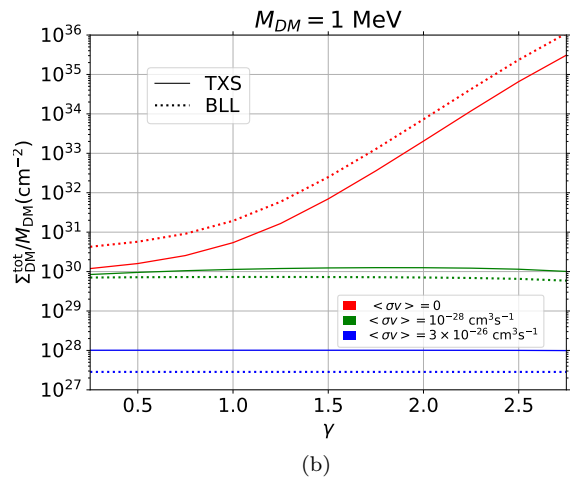
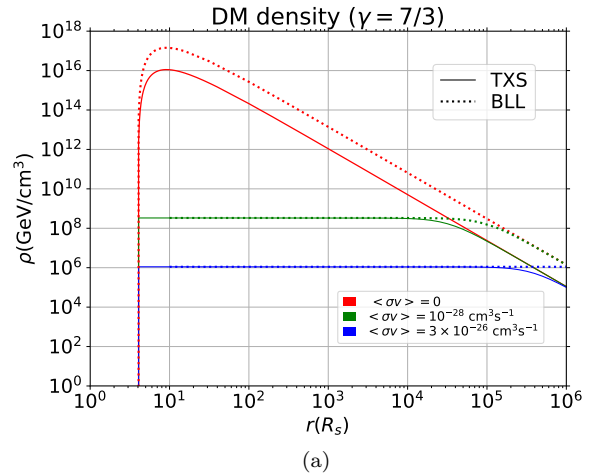


FIG. 1: DM density profile: (a) Variation in ρ_{DM} with distance from BH center (in terms of R_s) with $\gamma = 7/3$ for TXS 0506+56 and BL Lacertae shown by solid and dotted lines. (b) Variation of $\Sigma_{\text{DM}}^{\text{tot}}/m_{\chi}$ with γ for a fixed DM mass 1 MeV for the earlier mentioned two BHs. In both the plots the red, green and blue line correspond to the cases with $\langle \sigma v \rangle = 0, 10^{-28} \text{ cm}^3 \text{ s}^{-1}, 3 \times 10^{-26} \text{ cm}^3 \text{ s}^{-1}$.

flux is the line of sight integral of DM density defined as $\Sigma_{\text{DM}}(r) = \int_{4R_s}^r \rho(r') dr'$. $\Sigma_{\text{DM}}(r)$ saturates at $r \gtrsim 10^5 R_s$ and hence $\Sigma_{\text{DM}}^{\text{tot}} = \Sigma_{\text{DM}}(10^5 R_s)$ is used to define the total LOS integral as conventionally done in literature [31].

There are different other values of γ found in literature which may result in different density profiles [35, 51]. In Fig.1(b) we present the variation of $\Sigma_{\text{DM}}^{\text{tot}}/m_{\chi}$ with γ for a fixed DM mass 1 MeV for the earlier mentioned two BHs. The line type and colors follow the same convention as in Fig.1(a). Note that, the spike radius is controlled by the BH mass ($R_s \propto M_{\text{BH}}$) and hence it is larger for TXS 0506+56 than BL Lacertae due to the heavier mass of the former one. For the same reason normalization in density $\rho_1 (\propto M_{\text{BH}}^{-2})$ and $\Sigma_{\text{DM}}^{\text{tot}} (\propto M_{\text{BH}}^{-1})$ is smaller for TXS 0506+56 than BL Lacertae. This feature is reflected in

Fig.1(b) where BL Lacertae has larger LOS density for $\langle\sigma v\rangle = 0$. Note that for $\langle\sigma v\rangle \neq 0$ $\Sigma_{\text{DM}}^{\text{tot}}$ doesn't vary significantly with γ . However, for $\langle\sigma v\rangle = 0$, $\Sigma_{\text{DM}}^{\text{tot}}$ varies by order's of magnitude with γ . With an increase in γ the DM spike becomes steeper leading to higher density as reflected in the aforementioned plot. For a comparative analysis with existing literature [26, 31], in this work we pick two well studied profiles of the spike: $\gamma = 7/3$ [35] and $\gamma = 3/2$ [52]. The qualitative change in the direct search limits for other values of γ can be easily comprehended from the discussion above. Having a detailed discussion about the blazar jet and DM spike density we are now set to evaluate the boosted DM flux.

C. Flux of Boosted DM

As mentioned earlier, the high energy electrons from the blazar jet may up-scatter the surrounding DM particles. Since the DM particles have very small velocity $v \sim 10^{-3}c$ compared to blazar jet, DM can be treated as at rest. Upon scattering the differential flux of the incoming DM is given by [31],

$$\frac{d\phi_\chi}{dT_\chi} = \frac{\Sigma_{\text{DM}}^{\text{tot}}}{2\pi m_\chi d_L^2} \int_0^{2\pi} d\phi_s \int_{T_e^{\text{min}}}^{T_e^{\text{max}}} dT_e \frac{d\sigma_{\chi e}}{dT_\chi} \frac{d\Gamma_e}{dT_e d\Omega_e}. \quad (4)$$

ϕ_s is the azimuthal angle with respect to LOS. The cosine of the polar angle in observer frame (μ) is related to the cosine of the scattering angle ($\bar{\mu}$) corresponding to DM rest frame by a 2 dimensional rotation of angle θ_{LOS} given as [31],

$$\mu(\bar{\mu}, \phi_s) = \bar{\mu} \cos \theta_{\text{LOS}} + \sin \phi_s \sin \theta_{\text{LOS}} \sqrt{1 - \bar{\mu}^2}, \quad (5)$$

where, $\bar{\mu}$ is defined as [31],

$$\bar{\mu}(T_e, T_\chi) = \left[1 + \frac{T_\chi^{\text{max}} - T_\chi}{T_\chi} \frac{(m_\chi + m_e)^2 + 2m_\chi T_e}{(m_\chi + m_e + T_e)^2} \right]^{-1/2} \quad (6)$$

$T_\chi^{\text{max}} = (T_e^2 + 2m_e T_e)(T_e + (m_\chi + m_e)/(2m_\chi))^{-1}$ is the maximum kinetic energy obtained by DM upon scattering with e and $\mu_{\chi e}$ is the reduced mass of DM electron system.

Coming back to eq.(4), $T_e^{\text{min}}(T_\chi)$ is the minimum kinetic energy required to upscatter a non-relativistic DM to energy T_χ and is given by [20, 26],

$$T_e^{\text{min}} = \left(\frac{T_\chi}{2} - m_e \right) \left[1 \pm \sqrt{1 + \frac{2T_\chi(m_e + m_\chi)^2}{m_\chi(2m_e - T_\chi)^2}} \right], \quad (7)$$

where (+) or (-) sign is applicable when $T_\chi > 2m_e$ or $T_\chi < 2m_e$, respectively. However, according to the SED modeling [44, 45], the blazar jet itself has a cut off in the low energy $E'_{e,\text{min}} = m_e \gamma'_{e,\text{min}}$. Hence the lower cut off in the kinetic energy of jet electrons in rest frame is given by, $T_{e,\text{jet}}^{\text{min}} = m_e (\gamma'_{e,\text{min}} \Gamma_B^{-1} (1 - \beta_B \cos \theta_{\text{LOS}})^{-1} - 1)$.

Thus the lower limit of the above mentioned integration becomes $\text{Max}\{T_e^{\text{min}}, T_{e,\text{jet}}^{\text{min}}\}$. On the other hand, the upper cut off in the energy of the blazar jet sets the upper limit $T_{e,\text{jet}}^{\text{max}} = m_e (\gamma'_{e,\text{max}} \Gamma_B^{-1} (1 - \beta_B \cos \theta_{\text{LOS}})^{-1} - 1)$. Finally $d\sigma_{\chi e}/dT_\chi$ is the differential cross section of DM and incoming e . While computing $d\sigma_{\chi e}/dT_\chi$ the information about underlying particle physics model is important and will be discussed in the following sections.

Being upscattered DM particles may reach earth and the incoming high energy DM particles are expected to scatter with target electrons in the multi-ton neutrino detectors. The expected differential recoil rate is given by,

$$\frac{dR}{dE_R} = t_{\text{exp}} N_T \mathcal{E}(E_R) \int_{T_\chi^{\text{min}}(E_R)}^{\infty} \frac{d\Phi_\chi^{\text{tot}}}{dT_\chi} \frac{d\sigma_{\chi e}}{dE_R} dT_\chi, \quad (8)$$

where E_R is the recoil energy, t_{exp} is the time of exposure and N_T denotes the number of target particles. T_χ^{min} is the minimum kinetic energy of incoming DM particle to produce a recoil energy E_R which is given by [20, 26],

$$T_\chi^{\text{min}} = \left(\frac{E_R}{2} - m_\chi \right) \left[1 \pm \sqrt{1 + \frac{2E_R(m_e + m_\chi)^2}{m_e(2m_\chi - E_R)^2}} \right], \quad (9)$$

where (+) or (-) sign is applicable when $E_R > 2m_\chi$ or $E_R < 2m_\chi$, respectively. $\mathcal{E}(E_R)$ is the efficiency factor of the experiment. $d\sigma_{\chi e}/dE_R$ is the differential cross-section of incoming energetic χ and target e at rest.

III. ELECTROPHILIC DM

To evaluate the BBDM flux and expected DM signature one needs the information about the Lorentz structure of the presumed interaction between DM and SM. Thus it is crucial to consider at least a minimal effective DM model. In this section, we consider DM models that can allow interaction of DM with only e , which we refer as electrophilic DM.

A. ALP portal

We consider a minimum DM scenario coupled to a pseudo scalar dubbed as ALP like,

$$\mathcal{L} \supset ig_{a\chi} a \bar{\chi} \gamma^5 \chi + ig_{ae} a \bar{e} \gamma^5 e \quad (10)$$

Thus χ can scatter with ambient jet e through the ALP portal. The differential elastic cross section between χ and incoming e is given by,

$$\frac{d\sigma_{\chi e}}{dT_\chi} = \frac{1}{8\pi} \frac{g_{a\chi}^2 g_{ae}^2 m_\chi T_\chi}{(2m_e T_e + T_e^2)(m_a^2 + 2m_\chi T_\chi)^2}, \quad (11)$$

In Fig.2 we present the variation of differential flux

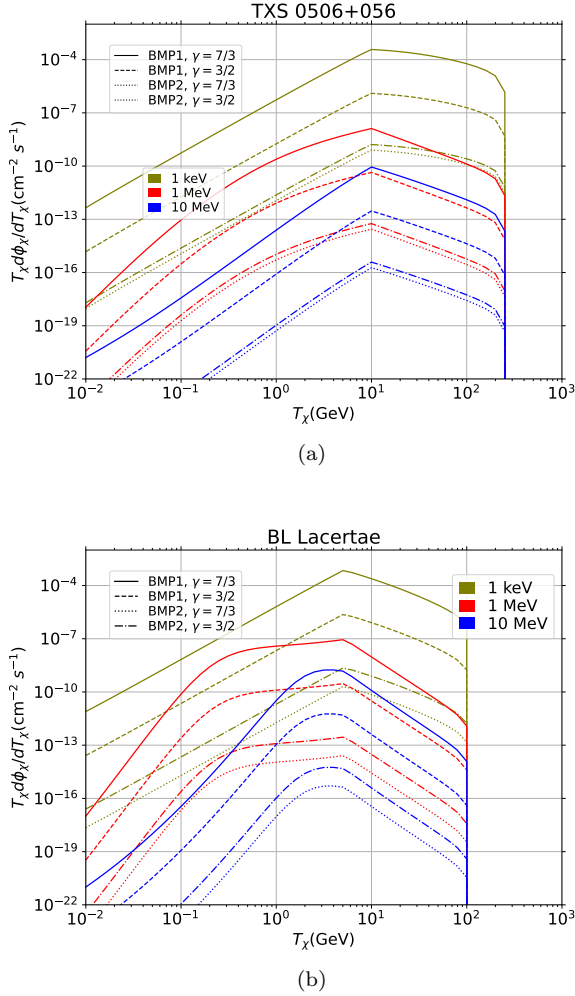


FIG. 2: Variation of differential flux of BBDM with T_χ for fixed values of $g_\chi g_e = 10^{-4}$, $m_a = 100$ MeV for (a) TXS 0506+056 and (b) BL Lacertae. The flux due to three different DM masses $m_\chi = 1$ keV, 1 MeV, 10 MeV are shown by olive, red and blue color respectively. The solid and dashed lines signify BMP1 with $\gamma = 7/3$ and $3/2$ respectively, whereas, the dashed dot and dotted lines signify BMP2 with $\gamma = 7/3$ and $3/2$ respectively.

of boosted DM using eq.(4) with T_χ for TXS 0506+056 (Fig.2(a)) and BL Lacertae (Fig.2(b)) for fixed values of $g_\chi g_e = 10^{-4}$, $m_a = 100$ MeV. we show the flux for three different DM masses $m_\chi = 1$ keV, 1 MeV, 10 MeV shown by olive, red and blue color respectively. Also we consider two benchmark points (BMP) for this plot: $\langle\sigma v\rangle = 0$ (BMP1) and $\langle\sigma v\rangle = 3 \times 10^{-26}$ cm³s⁻¹ (BMP2). The solid and dashed lines signify BMP1 with $\gamma = 7/3$ and $3/2$ respectively. On the other hand dashed dot and dotted lines signify BMP2 with $\gamma = 7/3$ and $3/2$ respectively. As expected with lower m_χ DM number density increases leading to higher DM flux and for both the blazar sources BMP1 results in higher DM flux for a fixed γ . The nonzero annihilation cross-section for BMP2 leads to a decrease

in the incoming DM flux. For same BMP $\gamma = 7/3$ results in higher flux than $\gamma = 3/2$ for higher LOS density (see Fig.1(b)). The sharp cut offs in high T_χ for both the blazar sources are the consequence of the upper limit on the blazar jet electron energy $T_{e,\text{jet}}^{\text{max}}$. The higher value of $\gamma'_{e,\text{max}}$ for TXS 0506+056 (Fig.2(a)) results in higher flux for $T_\chi \gtrsim 100$ GeV which will lead to more stringent constraint on DM parameter space as will be shown in the following discussion.

To evaluate the recoil rate in the detector we use eq.(8) with $d\sigma_{\chi e}/dE_R$ given by,

$$\frac{d\sigma_{\chi e}}{dE_R} = \frac{1}{8\pi} \frac{g_{a\chi}^2 g_{ae}^2 m_e E_R}{(2m_\chi T_\chi + T_\chi^2)(m_a^2 + 2m_e E_R)^2}. \quad (12)$$

For this work we consider Super Kamiokande (Super-K) as detector due to its larger target size $N_T = 7.5 \times 10^{33}$ with exposure time 2628.1 days [38]. We evaluate the DM signal in 3 different energy bins: 0.1-1.33 GeV (Bin 1), 1.33-20 GeV (Bin 2), 20-10³ GeV (Bin 3) following the approach developed in ref.[32]. For each bin the event rate, expected background and signal efficiency are provided in ref.[38]. Using the angular information of the incoming blazar jet the dominant atmospheric neutrino background can be vetoed. We use the statistical analysis performed in ref.[32] to draw the 95% confidence level (CL) upper limit for ALP mediated boosted DM electron cross-section.

Before delving into the results from Super-K we highlight the existing constraints on the light electrophilic mediator. For a mediator coupled with electrons stringent bounds come from several ground based experiments as well as from astrophysics. We enumerate them below. Though we specifically discuss here about ALP mediator, the process of obtaining the bounds and the qualitative features remain same for vector mediator as well.

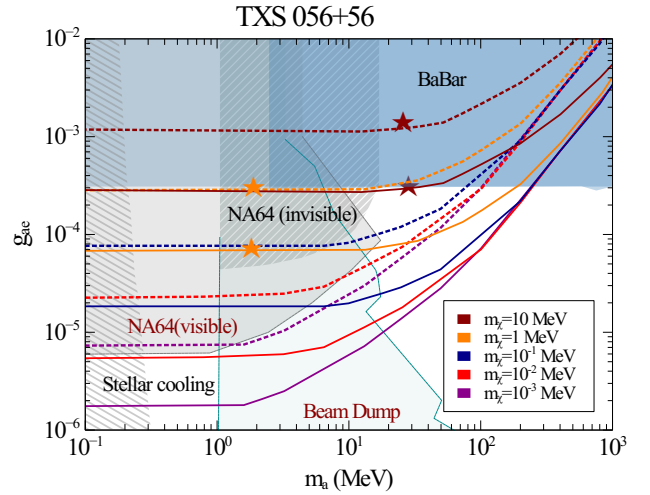
- **LEP:** Large electron positron collider (LEP) at CERN searches for missing energy through the process $e^+ + e^- \rightarrow \gamma + X$, X being the missing energy [53], and thus excludes $g_{ae} \gtrsim 2 \times 10^{-2}$ for $m_a > 2m_\chi$ [54].
- **BaBar:** BaBar also looks for missing energy through the same process as LEP does and places stringent constraint on $g_{ae} \gtrsim 3 \times 10^{-4}$ for m_a upto 10 GeV [42, 54–57].
- **NA64:** Though NA64 is one type of Beam Dump experiment, we discuss separately as it sets the most stringent limit on the parameter space relevant to us. In contrast to previous experiments NA64 looks for both visible and invisible decay of the mediator [43, 58]. Here high energy electron beam is dumped at target like $e^- + Z \rightarrow e^- + Z + a^*$, and then the mediator can decay either visibly or invisibly. In the visible channel ALP mediator can decay to SM particles (di-photon via loop for $m_a < 2m_e$) and no excess in observed data leads to

constraint on $g_{ae} \gtrsim 10^{-5}$ [59]. On the other hand the invisible decay sets limit for $1 \text{ MeV} < m_a < 15 \text{ MeV}$ for $m_a > 2m_\chi$ [43].

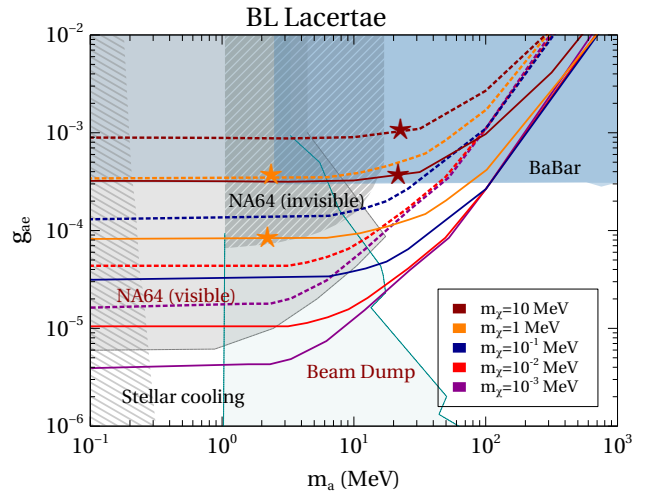
- **Beam Dump:** In this paper by “Beam Dump” we refer to other fixed target experiments looking for leptonic decay of the mediator through displaced vertex search like E137, E141, Orsay [60, 61, 61]. These experiments constrain roughly $g_{ae} \gtrsim 10^{-7}$ for $1 \text{ MeV} < m_a < 100 \text{ MeV}$ [62–65].
- **Astrophysical constraints:** The most studied astrophysical constraint on light mediator is from supernova cooling. Light mediators with mass $\lesssim \mathcal{O}(\text{MeV})$ can be produced in the core and with feeble interaction it may escape the core leading to cooling of supernova. The observation of SN1987A provides the information about the luminosity and constrains such energy loss placing constraint on g_{ae} [66]. However SN1987A bounds are disputed in literature due to the uncertainties associated with the progenitor [67]. Nevertheless these bounds are applicable to very small couplings ($g_{ae} \sim 10^{-7}$) compared to our region of interest. Recent study has also pointed out strong constraint on leptophilic scalar mediator mass upto $\sim 10 \text{ MeV}$ [68]. Translating these bounds for ALP mediator is beyond the scope of this work. However, even after considering this bound we still have sufficient parameter space for $m_a \gtrsim 10 \text{ MeV}$. Similarly other astrophysical bodies like red giant, white dwarf places constraint for $m_a \lesssim \mathcal{O}(1) \text{ keV}$ [69].

It is also worth discussing the dependence of the constraints on DM mass. For our minimal model the invisible decay constraints coming from BaBar, NA64 invisible are relevant as long as $m_a > 2m_\chi$ so that it can decay dominantly to dark sector as mentioned earlier. On the other hand the visible decay constraints (Beam Dump, NA64 visible) are derived assuming that the mediator decays to SM particles with 100% branching ratio (BR). To show the direct search limits on g_{ae} (Fig.3) in our analysis we consider the aggressive benchmark with $g_\chi = \sqrt{4\pi}$. Thus when $m_a > 2m_\chi$, ALP decays to dark sector with almost $\sim 100\%$ BR leading to very tiny room for visible decays and hence the visible decay constraints become negligible in that regime. This point is crucial in understanding our limits on BBDM from Super-K in Fig.3.

In Fig.3 we present the obtained limits on the blazar boosted DM in the mass vs. coupling parameter space of ALP mediator. For comparison we display the constraints from TXS 0506+56 (Fig.3(a)) and BL Lacertae (Fig.3(b)). Constraints with $\gamma = 7/3$ ($\gamma = 3/2$) are depicted by solid (dashed) lines. The region above individual colored lines are excluded from DM searches for different DM mass $m_\chi = 10 \text{ MeV}$, 1 MeV , 0.1 MeV , 10^{-2} MeV , 10^{-3} MeV denoted by brown, orange, blue, red and magenta colors respectively. We show the constraints assuming $\langle \sigma v \rangle = 0$ for both the blazar sources



(a)



(b)

FIG. 3: 95% CL Constraints on BBDM in m_a vs. g_{ae} parameter space along with other existing constraints on ALP. Region above the individual colored lines are excluded from DM searches for different DM mass $m_\chi = 10 \text{ MeV}$, 1 MeV , 0.1 MeV , 10^{-2} MeV , 10^{-3} MeV denoted by brown, orange, blue, red and magenta colored solid (dashed) lines for $\gamma = 7/3$ ($\gamma = 3/2$) respectively. The different shaded regions correspond to existing constraints on ALP discussed in the text. The colored “star” marks signify the lower limit on m_a of the BaBar constraint ($g_{ae} < 3 \times 10^{-4}$) for different DM masses.

to obtain an optimistic limit. In the same parameter space we also showcase current constraints from different searches of electrophilic ALP. For larger couplings constraints from BaBar [42, 54, 56, 57] is relevant shown by light blue shaded region. For ALP mass $\sim \mathcal{O}(1) \text{ MeV}$ constraints from different Beam Dump experiments (light cyan shaded region) [61–65], and NA64 invisible decay (solid grey region) [43, 58] set the most stringent limit. In the MeV-sub MeV region NA64 visible decay constraint

m_χ (MeV)	BaBar(MeV)	NA64 visible	NA64 invisible	Beam Dump	TXS	BLL
10	$20-15 \times 10^3$	$m_a < 20$ MeV	\times	\checkmark	12-20 MeV	12-20 MeV
1	$2-15 \times 10^3$	$m_a < 2$ MeV	$m_a > 2$ MeV	\times	30-80MeV	40-60MeV
10^{-1}	$0.2 - 15 \times 10^3$	\times	\checkmark	\times	0.3-110 MeV	0.3-90 MeV
10^{-2}	\checkmark	\times	\checkmark	\times	0.3-110 MeV	0.3-90 MeV
10^{-3}	\checkmark	\times	\checkmark	\times	0.3-110 MeV	0.3-90 MeV

TABLE II: Possible constraints and their range on m_a for different m_χ . The last two columns named “TXS” and “BLL” represent the range of m_a of the “new” parameter space probed by BBDM searches at Super-K assuming TXS 0506+56 (Fig.3(a)) and BL Lacertae (Fig.3(b)) as blazar source with $\gamma = 7/3$. Ticks refer to the constraints those are applicable to all the region as shown in the plot. Cross-mark signify that the respective constraint is not applicable.

[43, 58] is shown by backward diagonal grey region. Astrophysical constraints like stellar cooling is relevant in the sub-MeV region shown by forward diagonal light gray region [70].

For comparative analysis we plot all the limits for different m_χ in the same plane, although some of the existing constraints change with variation in DM mass as hinted earlier. The summary of relevant constraints for different DM masses are presented in Table II. For $m_\chi = 10$ MeV (brown line) and $m_\chi = 1$ MeV (orange line) BaBar excludes $g_{ae} > 3 \times 10^{-4}$ from $m_a \sim 15$ GeV

to only $m_a = 20$ MeV and $m_a = 2$ MeV respectively shown by the colored “star mark” on the individual limits. So, practically there is no limit from BaBar on the left side of the “star mark” for respective m_χ . Similarly the NA64 invisible decay constraint doesn’t apply for $m_\chi = 10$ MeV. On the other hand, “Beam Dump” constraints (visible) are applicable for only $m_\chi = 10$ MeV for our region of interest and not for other chosen DM masses. To signify the relevance of NA64 visible decay and Beam Dump constraints for only $m_\chi = 10$ MeV we show the labels in brown.

The strongest bound for ALP mediated DM electron cross-section comes from TXS 0506+56 (Fig.3(a)) with $\gamma = 7/3$. As discussed in context of Fig.2 that, $\gamma = 3/2$ leads to smaller DM flux than with $\gamma = 7/3$ for both the blazar sources, the bounds are more stringent for $\gamma = 7/3$. For, $m_a \sim 30-100$ MeV, $g_{ae} \lesssim 10^{-4}$ the parameter space remains allowed by all other existing searches. Considering ALP mediated DM, Super Kamiokande excludes these parameter spaces for $m_\chi \lesssim 10$ MeV. With decreasing DM mass the enhanced DM flux leads to more stringent constraint. For larger DM masses ($m_\chi \gtrsim 10$ MeV) the bounds obtained are already within existing constraints for $m_a \gtrsim m_\chi$ and hence can’t probe any new parameter space. For even lighter DMs ($m_\chi \leq 1$ MeV) the limits on the ALP mass-coupling parameter space goes through the region excluded by stellar cooling and NA64 invisible decay constraint. There is still lot of parameter space left un-excluded for $m_a \gtrsim 0.3$ MeV, $g_{ae} \lesssim 6 \times 10^{-4}$ which can be probed by this boosted DM with $m_\chi < 1$ MeV. We restrict our analysis for DM masses down to $m_\chi \geq 1$ keV, as lighter fermion DM is forbidden by Pauli exclusion principle [71]. The blazar-boosted DM flux from BL Lacertae has less kinetic energy than TXS 0506+56, leading to weaker constraints coming from the former one. Finally to draw the exclusion regions we assume $\langle \sigma v \rangle = 0$ which is realistic for the case of asymmetric DM [72]. However, the presence of a non zero annihilation of DM to SM or other dark sector particles may deplete the spike density and thereby weaken the

constraint. For example, with $\langle \sigma v \rangle = 10^{-28} \text{cm}^3 \text{s}^{-1}$ and $m_\chi = 1$ MeV, the LOS density drops by factor $\sim 10^3$ (see Fig.1(b)) which will weaken the constraint by factor ~ 6 since the rate depends on $\sim g_{ae}^4$. In such case new regions probed by BBDM become small. For our minimal scenario DM can annihilate to only e, a for $m_\chi > m_e, m_a$. In that case the constraints for heavier DM masses ($m_\chi \gtrsim 1$ MeV) are weakened due to less density. However, the constraints for $m_\chi \lesssim 10^{-1} \text{MeV} < m_a$ do not change at all for realistic cross-sections even in presence of a non zero annihilation and thus our bounds are robust in this sense.

B. Vector portal

Similarly one can consider a vector portal DM where the mediator couples to both DM and e like,

$$\mathcal{L} \supset g_{V\chi} V_\mu \bar{\chi} \gamma^\mu \chi + g_{Ve} V_\mu \bar{e} \gamma^\mu e. \quad (13)$$

V is the vector mediator with mass m_V and $g_{V\chi}, g_{Ve}$ are the corresponding coupling strength with χ, e . There are several well motivated gauge extension featuring such behavior [73]. As an example of UV completion of such scenario one may choose the well studied $L_e - L_\tau$ model, where apart from $e, \tau, \nu_{e,\tau}$ [74], DM χ also couples to the BSM gauge boson V [73]. The differential cross-section of DM with high energy jet electron is given by,

$$\frac{d\sigma_{\chi e}}{dE_R} = \frac{1}{4\pi} \frac{g_{V\chi}^2 g_{Ve}^2}{(2m_e T_e + T_e^2)(m_V^2 + 2m_\chi T_\chi)^2} \times (2m_\chi(m_i + T_i)^2 - T_\chi((m_e + m_\chi)^2 + 2m_\chi T_e) + m_\chi T_\chi^2), \quad (14)$$

And the differential recoil cross-section is given by,

$$\frac{d\sigma_{\chi e}}{dT_\chi} = \frac{1}{4\pi} \frac{g_{V\chi}^2 g_{Ve}^2}{(2m_\chi T_\chi + T_\chi^2)(m_V^2 + 2m_e T_e)^2} \times (2m_i(m_\chi + E_R)^2 - E_R((m_i + m_\chi)^2 + 2m_i T_\chi) + m_i E_R^2). \quad (15)$$

Following the same approach as in the previous subsection we evaluate the event rate at Super-K and display the constraints on BBDM in Fig.4. We show the constraints in the m_V vs. g_{Ve} plane assuming TXS 0506+56 as blazar source. Though we do not show the bounds assuming BL Lacertae as blazar source, from our observation in earlier subsection we expect qualitatively similar or slightly weaker constraints from it. We show the limits on BBDM assuming $\gamma = 7/3$ ($\gamma = 3/2$) with solid (dashed) lines for different DM mass $m_\chi = 10$ MeV, 1 MeV, 0.1 MeV, 10^{-2} MeV, 10^{-3} MeV following the same color convention as in the earlier sub-section. Here also we consider $\langle\sigma v\rangle = 0$ to obtain the limits.

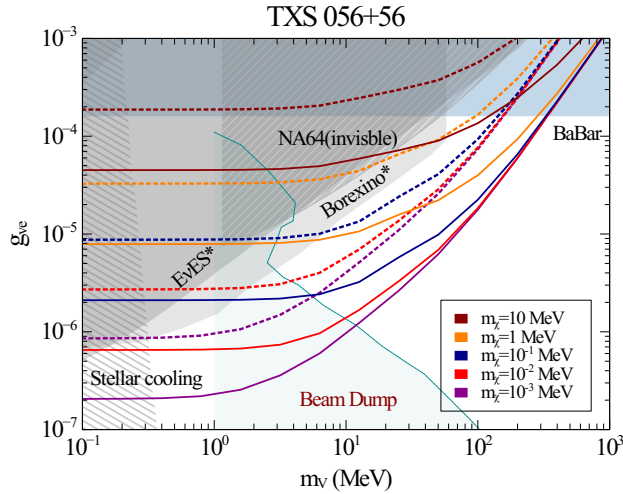


FIG. 4: 95% CL constraints on BBDM in m_V vs. g_{Ve} parameter space along with other existing constraints on electrophilic mediator. Region above the individual colored lines are excluded from DM searches for different DM mass $m_\chi = 10$ MeV, 1 MeV, 0.1 MeV, 10^{-2} MeV, 10^{-3} MeV denoted by brown, orange, blue, red and magenta colored solid (dashed) lines for $\gamma = 7/3$ ($\gamma = 3/2$) respectively. The different shaded regions correspond to existing constraints on ALP discussed in the text. The constraints with “star” in label signify that they are applicable when the mediator couples to neutrino as well e.g. in $L_e - L_\tau$ model.

In the same plane (Fig.4) we showcase other existing constraints on electrophilic vector mediators. As shown earlier, Babar ($g_{Ve} \gtrsim 10^{-4}$) [55, 75] and NA64 “invisible” [76] place strongest constraints on couplings with

higher strength. On the other hand, for lower values of the coupling, bounds from beam dump experiments [75] are applicable. Constraints from stellar cooling are applicable for $m_V \lesssim 0.4$ MeV [77]. Even though we do not mention explicitly in the plot, the invisible decay constraints (BaBar, NA64) are relevant as long as $m_a > 2m_\chi$ and visible decay constraints (Beam Dump) are applicable for only $m_a < 2m_\chi$ as elaborated earlier in detail. If the vector couples to neutrinos e.g. in models like $L_e - L_\tau$ [78], then neutrino scattering constraints from E ν ES from XENON [79, 80], Borexino [74, 81, 82] provides the strongest constraint. Despite all the stringent constraints the limits set by BBDM search exclude significant portion of new parameter space for $m_\chi \lesssim 10$ MeV. These constraints are significantly stronger than cosmic ray boosted DM search [30]. Although effective vector portal (without $\nu - V$ couplings) blazar boosted DM at heavy mediator limit has been investigated earlier in ref.[26], here we obtain the bounds in the whole mass vs. coupling plane of the mediator. In the absence of neutrino coupling of the mediator, BBDM explores new parameter space in the light mediator regime too as shown in Fig.4. Note that for vector mediator there is no momentum suppression in the cross-section which makes the limit on the coupling almost $\mathcal{O}(1)$ order (cross-section $\sim \mathcal{O}(10^4)$) stronger than ALP mediated scenario. Before concluding the discussion we highlight that the cosmological constraint on relativistic degrees of freedom N_{eff} excludes electrophilic mediators with mass $\lesssim \mathcal{O}(1)$ MeV and coupling $\gtrsim 10^{-9}$ [78, 83]. Our exclusion limits probe new parameter space despite of these constraints too. N_{eff} also excludes thermal DM for mass $\lesssim 3$ MeV [84]. However, such constraints are dependent on the underlying UV complete DM models, and can be subjugated by considering an extended dark sector. Thus blazar boosted scenario not only sets the strongest direct search limit in the (sub) MeV DM masses, rather it probes previously unconstrained parameter space for different mediators contrary to other boosted DM scenarios.

IV. DM WITH BOTH NUCLEON AND ELECTRON COUPLING

So far we discussed about DM that is boosted by only blazar electron jet. However, there exist several well motivated mediators that couple to both electron and proton (quarks), so that DM can be potentially up-scattered by both electron and protons in the blazar jet. The minimal and maximal boost factor of proton jet in the blob frame given by SED modeling are $\gamma'_{\min,p} = 1.0$ and $\gamma'_{\max,p} = 5.5 \times 10^7$ (way larger than electrons) for TX056+56 [32]. The gain in DM being up-scattered by proton as well is that boosted DM can now have higher flux even at energy $\sim 10^3$ GeV contrary to the electrophilic case [32]. Thus considering both the effects of proton and electron may lead to higher flux of BBDM resulting in more stringent bounds. To obtain the blazar proton jet of TX056+56 we use the same eq.(2) with the obvious replacements ($i \equiv p$): $m_e \rightarrow m_p$, $\alpha_e \rightarrow \alpha_p (= 2)$, and $L_e \rightarrow L_p (= 2.55 \times 10^{48}$ erg/s) [32]. The normalization constant c_e is also replaced by c_p normalized with respect to L_p .

A. ALP portal

For ALP portal DM scenario we consider the yukawa like couplings of ALP with quarks and electrons.

$$\mathcal{L} \supset \sum_{f=q,e} i \frac{c}{f_a} m_f a \bar{f} \gamma^5 f, \quad (16)$$

where, the sum is over quarks and electron. This type of lagrangian is motivated from DFSZ models [40]. For calculating DM up-scattering by electrons we use the same eq.(11) with $g_{ae} = \frac{c}{f_a} m_f$. While for the case of proton up-scattering we replace g_{ae} by $g_{ap} \approx 0.45 c/f_a m_u (m_p/(m_u + m_d))$ and multiply the whole equation with the square of a form factor given by, $F_a(q^2) = F_{\text{axial}}(q^2) C_q / (q^2 + M_q^2)$, with $C_q = 0.9$, $M_q = 0.33$ GeV, and $F_{\text{axial}}(q^2) = 1/(1 + q^2/\Lambda_a^2)^2$ ($\Lambda_a = 1.32$ GeV) [85]. To evaluate the incoming BBDM flux we add up both the contribution from electron and proton up-scattering [32]. While computing the recoil rate, we consider only electron scattering for conservative estimations since, with TeV energy and feeble couplings DM-proton scattering will be suppressed in the detector. We show the constraints on m_a vs. c/f_a plane in Fig. 5 and to signify the limits we follow the same convention as earlier used in this paper. Note that, the mass suppression in the aforementioned Yukawa like interaction makes the limits look apparently weaker than pure electrophilic case. One may recast the bound on $g_{ae} (= m_e c/f_a)$ as well and perceive that limits on the effective couplings are way stronger than the electrophilic case (5). Due to the presence of quark couplings strong constraints come from meson decay (invisible) in the low m_a regime shown by the gray shaded region (Charm) and light gray diagonal

shaded region ($B \rightarrow K + \text{invisible}$) [86]. In the high mass regime there exists constraint from BaBar [86]. Recall that these are invisible decay constraints and applicable for only $m_a > 2m_\chi$. On the other hand the beam dump constraints [60] are relevant for only $m_a < 2m_\chi$. For the same reasons kaon decay (to $e^+e^-/\mu^+\mu^-$) constraints are not applicable for our concerned parameter space [40]. Despite all these stringent constraints there still remains some open parameter space at $m_a \sim 200 - 400$ MeV which is constrained by BBDM searches assuming our minimal scenario.

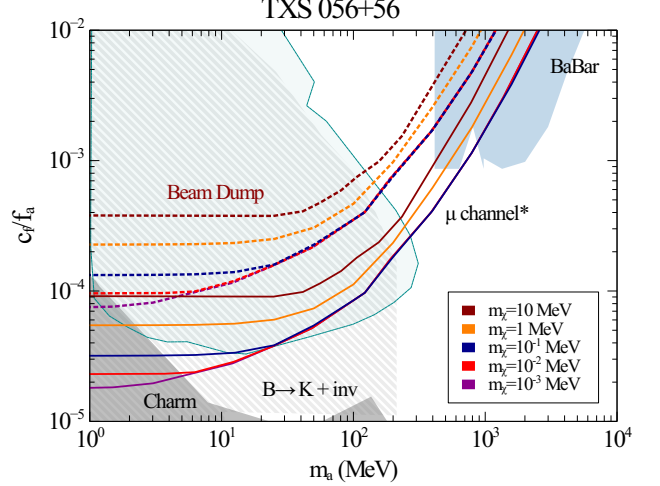


FIG. 5: 95% CL constraints on BBDM in m_a vs. c_f/f_a parameter space along with other existing constraints on ALP. Region above the individual colored lines are excluded from DM searches for different DM mass $m_\chi = 10$ MeV, 1 MeV, 0.1 MeV, 10^{-2} MeV, 10^{-3} MeV denoted by brown, orange, blue, red and magenta colored solid (dashed) lines for $\gamma = 7/3$ ($\gamma = 3/2$) respectively. The different shaded regions correspond to existing constraints on ALP discussed in the text.

To show the constraints in terms of electron and proton couplings, one may also assume effective ALP couplings like $\mathcal{L} \sim i g_{ae} a \bar{e} \gamma^5 e + i g_{ap} a \bar{p} \gamma^5 p$ being agnostic about the origin. The constraints on BBDM indeed explore some new parameter space in g_{ap} vs. g_{ae} plane for fixed m_a as shown in Fig.6 for $\gamma = 7/3$. We show the result for a fixed ALP mass $m_a = 0.5$ MeV along with the existing constraints on the couplings [29, 65]. While considering effective proton coupling of ALP there is an window of unconstrained region around $0.4 \text{ MeV} \lesssim m_a \lesssim 1 \text{ MeV}$ [29] which also remains un-excluded for electron coupling. The direct search constraints on BBDM is shown in the same plane with different lines for $m_\chi \in 10^{-3}, 10^{-2}, 10^{-1}, 1$ MeV shown by magenta, red, blue and orange color respectively. The regions above the contour lines are excluded from Super-K. For $g_{ap} \gtrsim 10^{-4}$ the region is excluded by meson invisible decay (for $m_a \leq 0.1$ MeV) and $g_{ap} \lesssim 2 \times 10^{-5}$ is excluded by supernova cooling [29]. NA64 visible decay constraint on $g_{ae} < 2 \times 10^{-6}$ is applicable to only $m_\chi = 1$ MeV. For smaller values of

$g_{ap} (\lesssim 10^{-6})$, the constraints are independent of g_{ap} and hence the limits become flat. Considering higher values of proton coupling ($g_{ap} \gtrsim 10^{-6}$) indeed sets stronger limit on g_{ae} as well which explore previously un-excluded parameter space.

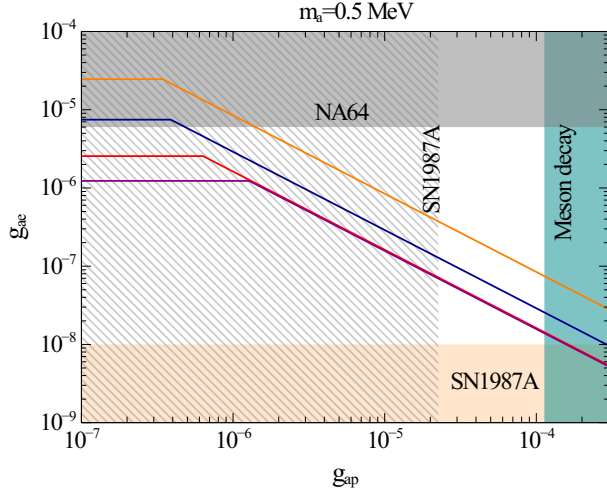


FIG. 6: 95% CL constraints on BBDM in g_{ap} vs. g_{ae} plane for fixed $m_a = 0.5$ MeV for $\gamma = 7/3$ considering TXS 056+56 as blazar source. Shaded regions correspond to the existing constraints on the couplings. Limits corresponding to $m_\chi \in 10^{-3}, 10^{-2}, 10^{-1}, 1$ MeV are shown by magenta, red, blue and orange color respectively.

B. Vector portal

Similarly, one may consider a vector like mediator which couples to both nucleon and electrons as in $B-L$ gauge extension [82]. In such scenario the gauge boson couples as

$$\mathcal{L} \supset \sum_{f=q,e} g_{B-L} q_f \bar{f} \gamma^\mu f V_\mu, \quad (17)$$

where, the sum is over quarks and electron. q_f is the $B-L$ gauge charge and $q_f = -1$ ($1/3$) for leptons (quarks). The coupling with DM is same as in eq.(13). For calculating DM up-scattering by electrons we use the same eq.(14) with $g_{ae} = g_{B-L}$. While for the case of proton we replace $g_{ap} = g_{B-L}$ and multiply the whole equation with the square of a form factor given by, $F_V(q^2) = (1+q^2/\Lambda_V^2)^{-2}$, with $\Lambda_V = 0.77$ GeV [30]. Analogous to previous section we add up the incoming BBDM flux due to both proton and electron up-scattering.

Finally from Super-K we place the 95% exclusion region in the m_V vs. g_{B-L} plane for different DM mass following the same color convention as used earlier in Fig.7. In the same plane we display the existing constraints from beam dump experiments [75], neutrino scattering constraints from $E\nu$ ES and $CE\nu$ NS in XENON

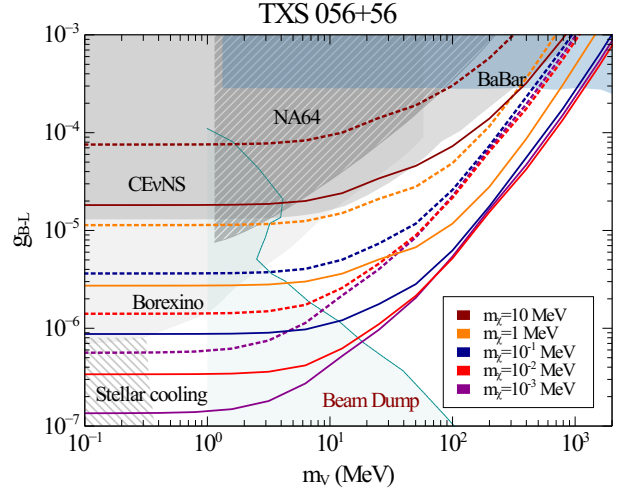


FIG. 7: 95% CL constraints on BBDM in m_V vs. g_{B-L} parameter space along with other existing constraints on $B-L$ gauge mediator. Region above the individual colored lines are excluded from DM searches for different DM mass $m_\chi = 10$ MeV, 1 MeV, 0.1 MeV, 10^{-2} MeV, 10^{-3} MeV denoted by brown, orange, blue, red and magenta colored solid (dashed) lines for $\gamma = 7/3$ ($\gamma = 3/2$) respectively. The different shaded regions correspond to existing constraints on ALP discussed in the text.

[79, 80], Borexino [74, 81, 82] and stellar cooling [77]. Despite all the stringent constraints the limits set by BBDM search exclude significant portion of new parameter space for $m_\chi \lesssim 10$ MeV. Since the DM flux is higher due to proton scattering compared to the electrophilic case, in the heavy mediator limit the constraints on the coupling g_{B-L} are almost 4 times stronger than in Fig.4 and hence the bounds on the cross-sections ($\sim g_{B-L}^2$) will be almost $\gtrsim \mathcal{O}(1)$ stronger. Thus combining both the effect of electrons and protons from blazar source can lead to stronger limits on MeV DM beyond the existing constraints on the mediator.

V. CONCLUSION

Multi-ton direct detection experiments face severe challenge to detect low mass galactic DM even with cutting edge instruments and large detector volume. To circumvent this issue one may adopt the boosted DM scenario which can potentially exclude the previously un-explored DM mass region. Generally significant portion of the exclusion limits obtained in such scenario may lie already within the existing constraints once we BSM mediators as a portal between DM and SM. The situation is even more disappointing for pseudoscalar mediators where the momentum suppression leads to very weak constraints on the cross-section. Such exclusion limits fails to explore any new parameter space and almost touches the unitarity limit in the mass-coupling parameter space of

the mediator [29]. This issue can be disentangled by considering low mass DM boosted by blazar jet which serves as the main goal of this work. We embark on a minimal BSM model, where a DM χ couples to SM via a pseudoscalar mediator, the so called ‘‘ALP portal DM’’. We estimate the expected recoil rate in Super Kamiokande triggered by such blazar boosted DM for different model parameters. For comparison we consider two benchmark blazar sources: TXS 0506+56 and a less distant BL Lacertae. The spike density of DM and blazar electron jet (with maximum energy $\sim 10^4$ GeV) leads to a significant amount of BBDM flux reaching at earth despite their large distances. We obtain 95% CL upper limit on DM- e interaction in the mass vs. coupling parameter space of the mediator ALP. Stringent constraints on the ALP parameter space arise from astrophysics and ground based searches like BaBar, NA64 and beam dump experiments, yet our limits exclude significant new parameter space ($g_{ae} \gtrsim 10^{-4}$ (2×10^{-5}) for $m_\chi = 1$ MeV (0.1 MeV) with $m_a/m_\chi = 10$). For completeness we also consider vector portal DM model and the BBDM search sets stronger limits on the mass vs. coupling plane ($g_{aV} \gtrsim 10^{-5}$ (2×10^{-6}) for $m_\chi = 1$ MeV (0.1 MeV) with $m_a/m_\chi = 10$) compared to other BDM scenarios investigated in the literature. Finally we allow the mediators to couple with both electron and nucleon for both ALP and vector portal DM scenario. Thanks to the higher kinetic energy (maximum energy $\sim 10^7$ GeV) of blazar protons, these type of interactions lead to further improvement in the sensitivity of BBDM searches at Super-K. We find that even smaller values of BSM couplings responsible for the interaction between low mass DM and SM can be probed combining the effect of multiple sources for DM up-scattering (i.e. both blazar electron and proton jets). Such characteristics are quite generic for models featuring a mediator with universal couplings to SM sector [40, 87]. One can explore the uncharted territories of light DM phenomenology with blazar boosted scenario considering concrete UV complete (low mass) DM models. Upon successful identifications of proper background, experiments like IceCube and future experiments like DUNE, JUNO have the potential to probe even smaller interaction strength between the dark and visible sectors.

Acknowledgment

We would like to thank Dilip K. Ghosh and Filippo Sala for the careful reading of the manuscript and the helpful comments. We also thank Rohan Pramanick, Pratick Sarkar for fruitful discussions and Gonzalo Herrera for the useful email conversations. It is our pleasure to thank Vikramaditya Mondal for providing computational support. We acknowledge the local hospitality at ICTS Bengaluru during the visit for GWBSM 76 program. This work is funded by CSIR, Government of India under the NET JRF fellowship scheme with Award file No. 09/080(1172)/2020-EMR-I.

Appendix A: Energy spectrum in observer’s frame

Following our discussion earlier in Sec.II A we consider the particles are going outwards in the blob frame with velocity β' and an angle θ' with respect to the z axis. The velocities of the jet particles in blob frame in parallel direction and perpendicular direction are given by proper Lorentz transformation,

$$\beta'_{\parallel} = \frac{\beta \cos \theta - \beta_B}{1 - \beta_B \beta \cos \theta}, \quad \beta'_{\perp} = \frac{\beta \sin \theta}{\Gamma_B (1 - \beta_B \beta \cos \theta)}. \quad (\text{A1})$$

Thus one can obtain the total velocity β' in terms of the two components and the boost factor $\gamma' = E'/m = (1 - \beta'^2)^{-1/2}$ in the blob frame can be found as,

$$\gamma' = \gamma \Gamma_B (1 - \beta_B \beta \cos \theta), \quad (\text{A2})$$

where, $\gamma = E/m$ is the boost factor in the observer frame. Another important quantity required to estimate the flux is the polar angle θ (in observer frame), which can be related to the polar angle θ' (in blob frame by) as,

$$\cos \theta' = \frac{(\beta \cos \theta - \beta_B)}{[(1 - \beta \beta_B \cos \theta)^2 - (1 - \beta^2)(1 - \beta_B^2)]^{1/2}}, \quad (\text{A3})$$

using the same eq.(A1).

For the sake of simplicity we define $\mu = \cos \theta$, and $\mu' = \cos \theta'$. The number of particle emitted from the blazar in per unit time / unit energy and unit solid angle is defined in the blob frame as $d\Gamma'/dE'd\Omega'$. Analogously the spectrum in observer frame is defined as,

$$\frac{d\Gamma}{dE d\Omega} = \Gamma_B \frac{d\Gamma'}{dE' d\Omega'} \left| \frac{\partial(E', \mu')}{\partial(E, \mu)} \right|, \quad (\text{A4})$$

where the second term is the Jacobian of the transformation J and can be obtained using eq.(A2)-eq.(A3). After some cumbersome algebra with the determinant one finds,

$$\frac{d\Gamma}{dE d\Omega} = \frac{d\Gamma'}{dE' d\Omega'} \times \frac{\beta \mu - \beta_B}{\sqrt{(1 - \beta_B \beta \mu)^2 - (1 - \beta^2)(1 - \beta_B^2)}}. \quad (\text{A5})$$

Normalization:

The normalization constant in eq.(2) is evaluated by normalizing the total luminosity in the observer’s frame with the observed one L_i (for particle i).

$$L_i = \int dE d\Omega \frac{d\Gamma_i}{dE_i d\Omega} E \quad (\text{A6})$$

However, looking at the expression of the spectrum it is expected that the integration is easier in blob frame. So,

using the jacobians we recast the integrand in the blob frame as,

$$L_i = \int dE' \frac{d\Gamma'_i}{dE'_i d\Omega'} E'_i d\Omega' \frac{1}{(1 - \beta_B \beta \cos \theta)}.$$

Since most of the emitted particles are relativistic we can assume $\beta \approx 1$ and inverting eq.(A3) we get

$$\cos \theta = \frac{\cos \theta' + \beta_B}{1 + \beta_B \cos \theta'}, \text{ and } 1 - \beta_B \cos \theta = \frac{1 - \beta_B^2}{1 + \beta_B \cos \theta'}$$

Substituting this in the above expression of L_i we get,

$$\begin{aligned} L_i &= \int dE' \frac{d\Gamma'_e}{dE'_e d\Omega'} E'_e d\Omega' \frac{1 + \beta_B \cos \theta'}{1 - \beta_B^2} \\ &= 2\pi \frac{1}{1 - \beta_B^2} 2 \frac{1}{4\pi} \int dE' \left(\frac{E'}{m_i}\right)^{-\alpha_i} E' \\ &= \Gamma_B^2 m_i^2 \int_{\gamma_{\min}}^{\gamma_{\max}} d\gamma' (\gamma')^{-\alpha_i} \end{aligned}$$

Hence one can find the normalization constant,

$$c_i = \frac{L_i}{\Gamma_B^2 m_i^2} \quad (\text{A7})$$

$$\times \begin{cases} 1/(\log(\gamma'^{\max}/\gamma'^{\min})) & \text{if } \alpha_i = 2 \\ \frac{1}{[(\gamma'_{\max})^{2-\alpha_i} - (\gamma'_{\min})^{2-\alpha_i}]} & \text{if } \alpha_i \neq 2 \end{cases}$$

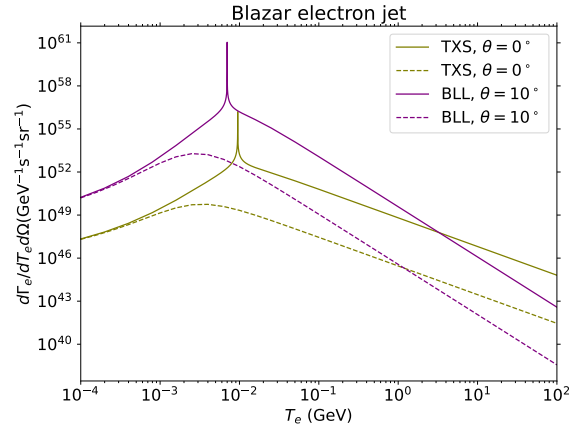


FIG. 8: Blazar electron jet flux for TXS 0506+56 (BL Lacertae) are shown with olive (magenta) color for two different values of $\theta(\cos^{-1} \mu) = 0^\circ, 10^\circ$ shown by solid and dashed lines respectively.

The corresponding blazar electron jet flux in observer's frame for the aforementioned two blazar source is shown in Fig.8. The flux due to TXS 0506+56 (BL Lacertae) are shown with olive (magenta) color for two different values of $\theta(\cos^{-1} \mu) = 0^\circ, 10^\circ$ depicted by solid and dashed lines respectively.

-
- [1] F. Zwicky, *Die Rotverschiebung von extragalaktischen Nebeln*, *Helv. Phys. Acta* **6** (1933) 110.
- [2] V.C. Rubin and W.K. Ford, Jr., *Rotation of the Andromeda Nebula from a Spectroscopic Survey of Emission Regions*, *Astrophys. J.* **159** (1970) 379.
- [3] PAMELA collaboration, *The cosmic-ray electron flux measured by the PAMELA experiment between 1 and 625 GeV*, *Phys. Rev. Lett.* **106** (2011) 201101 [1103.2880].
- [4] PLANCK collaboration, *Planck 2018 results. VI. Cosmological parameters*, *Astron. Astrophys.* **641** (2020) A6 [1807.06209].
- [5] R.J. Scherrer and M.S. Turner, *On the Relic, Cosmic Abundance of Stable Weakly Interacting Massive Particles*, *Phys. Rev. D* **33** (1986) 1585.
- [6] G. Jungman, M. Kamionkowski and K. Griest, *Supersymmetric dark matter*, *Phys. Rept.* **267** (1996) 195 [hep-ph/9506380].
- [7] M. Cirelli, A. Strumia and J. Zupan, *Dark Matter*, **2406.01705**.
- [8] G. Arcadi, M. Dutra, P. Ghosh, M. Lindner, Y. Mambrini, M. Pierre et al., *The waning of the WIMP? A review of models, searches, and constraints*, *Eur. Phys. J. C* **78** (2018) 203 [1703.07364].
- [9] J.L. Feng, *Dark Matter Candidates from Particle Physics and Methods of Detection*, *Ann. Rev. Astron. Astrophys.* **48** (2010) 495 [1003.0904].
- [10] T. Lin, *Dark matter models and direct detection*, *PoS* **333** (2019) 009 [1904.07915].
- [11] XENON collaboration, *Search for New Physics in Electronic Recoil Data from XENONnT*, *Phys. Rev. Lett.* **129** (2022) 161805 [2207.11330].
- [12] XENON collaboration, *First Dark Matter Search with Nuclear Recoils from the XENONnT Experiment*, *Phys. Rev. Lett.* **131** (2023) 041003 [2303.14729].
- [13] LZ collaboration, *Search for new physics in low-energy electron recoils from the first LZ exposure*, *Phys. Rev. D* **108** (2023) 072006 [2307.15753].
- [14] LZ COLLABORATION collaboration, *Dark Matter Search Results from 4.2 Tonne-Years of Exposure of the LUX-ZEPLIN (LZ) Experiment*, **2410.17036**.
- [15] PANDAX-II collaboration, *Results of dark matter search using the full PandaX-II exposure*, *Chin. Phys. C* **44** (2020) 125001 [2007.15469].
- [16] LUX collaboration, *Results from a search for dark matter in the complete LUX exposure*, *Phys. Rev. Lett.* **118** (2017) 021303 [1608.07648].
- [17] DEAP collaboration, *Search for dark matter with a 231-day exposure of liquid argon using DEAP-3600 at SNOLAB*, *Phys. Rev. D* **100** (2019) 022004 [1902.04048].
- [18] DARKSIDE collaboration, *DarkSide-50 532-day Dark*

- Matter Search with Low-Radioactivity Argon, *Phys. Rev. D* **98** (2018) 102006 [1802.07198].
- [19] W. Yin, *Highly-boosted dark matter and cutoff for cosmic-ray neutrinos through neutrino portal*, *EPJ Web Conf.* **208** (2019) 04003 [1809.08610].
- [20] T. Bringmann and M. Pospelov, *Novel direct detection constraints on light dark matter*, *Phys. Rev. Lett.* **122** (2019) 171801 [1810.10543].
- [21] A. Das and M. Sen, *Boosted dark matter from diffuse supernova neutrinos*, *Phys. Rev. D* **104** (2021) 075029 [2104.00027].
- [22] D. Ghosh, A. Guha and D. Sachdeva, *Exclusion limits on dark matter-neutrino scattering cross section*, *Phys. Rev. D* **105** (2022) 103029 [2110.00025].
- [23] Y. Ema, F. Sala and R. Sato, *Light Dark Matter at Neutrino Experiments*, *Phys. Rev. Lett.* **122** (2019) 181802 [1811.00520].
- [24] T.N. Maity and R. Laha, *Cosmic-ray boosted dark matter in Xe-based direct detection experiments*, *Eur. Phys. J. C* **84** (2024) 117 [2210.01815].
- [25] V. De Romeri, A. Majumdar, D.K. Papoulias and R. Srivastava, *XENONnT and LUX-ZEPLIN constraints on DSNB-boosted dark matter*, *JCAP* **03** (2024) 028 [2309.04117].
- [26] D. Bardhan, S. Showmick, D. Ghosh, A. Guha and D. Sachdeva, *Bounds on boosted dark matter from direct detection: The role of energy-dependent cross sections*, *Phys. Rev. D* **107** (2023) 015010 [2208.09405].
- [27] J.B. Dent, B. Dutta, J.L. Newstead and I.M. Shoemaker, *Bounds on Cosmic Ray-Boosted Dark Matter in Simplified Models and its Corresponding Neutrino-Floor*, *Phys. Rev. D* **101** (2020) 116007 [1907.03782].
- [28] Y. Ema, F. Sala and R. Sato, *Neutrino experiments probe hadrophilic light dark matter*, *SciPost Phys.* **10** (2021) 072 [2011.01939].
- [29] N.F. Bell, J.L. Newstead and I. Shaukat-Ali, *Cosmic-ray boosted dark matter confronted by constraints on new light mediators*, *Phys. Rev. D* **109** (2024) 063034 [2309.11003].
- [30] A. Guha and J.-C. Park, *Constraints on cosmic-ray boosted dark matter with realistic cross section*, *JCAP* **07** (2024) 074 [2401.07750].
- [31] J.-W. Wang, A. Granelli and P. Ullio, *Direct Detection Constraints on Blazar-Boosted Dark Matter*, *Phys. Rev. Lett.* **128** (2022) 221104 [2111.13644].
- [32] A. Granelli, P. Ullio and J.-W. Wang, *Blazar-boosted dark matter at Super-Kamiokande*, *JCAP* **07** (2022) 013 [2202.07598].
- [33] C.M. Urry and P. Padovani, *Unified schemes for radio-loud active galactic nuclei*, *Publ. Astron. Soc. Pac.* **107** (1995) 803 [astro-ph/9506063].
- [34] A.A. Abdo, M. Ackermann, I. Agudo, M. Ajello, H.D. Aller, M.F. Aller et al., *The spectral energy distribution offermibright blazars*, *The Astrophysical Journal* **716** (2010) 30–70.
- [35] P. Gondolo and J. Silk, *Dark matter annihilation at the galactic center*, *Phys. Rev. Lett.* **83** (1999) 1719 [astro-ph/9906391].
- [36] S. Showmick, D. Ghosh and D. Sachdeva, *Blazar boosted dark matter — direct detection constraints on $\sigma\epsilon$: role of energy dependent cross sections*, *JCAP* **07** (2023) 039 [2301.00209].
- [37] A.G. De Marchi, A. Granelli, J. Nava and F. Sala, *Did IceCube discover Dark Matter around Blazars?*, **2412.07861**.
- [38] SUPER-KAMIOKANDE collaboration, *Search for Boosted Dark Matter Interacting With Electrons in Super-Kamiokande*, *Phys. Rev. Lett.* **120** (2018) 221301 [1711.05278].
- [39] R.D. Peccei and H.R. Quinn, *CP Conservation in the Presence of Instantons*, *Phys. Rev. Lett.* **38** (1977) 1440.
- [40] A. Bharucha, F. Brümmer, N. Desai and S. Mutzel, *Axion-like particles as mediators for dark matter: beyond freeze-out*, *JHEP* **02** (2023) 141 [2209.03932].
- [41] D.K. Ghosh, A. Ghoshal and S. Jeessun, *Axion-like particle (ALP) portal freeze-in dark matter confronting ALP search experiments*, *JHEP* **01** (2024) 026 [2305.09188].
- [42] M. Bauer, M. Neubert and A. Thamm, *Collider Probes of Axion-Like Particles*, *JHEP* **12** (2017) 044 [1708.00443].
- [43] NA64 collaboration, *Search for pseudoscalar bosons decaying into e^+e^- pairs in the NA64 experiment at the CERN SPS*, *Phys. Rev. D* **104** (2021) L111102 [2104.13342].
- [44] M. Cerruti, A. Zech, C. Boisson, G. Emery, S. Inoue and J.P. Lenain, *Leptohadronic single-zone models for the electromagnetic and neutrino emission of TXS 0506+056*, *Mon. Not. Roy. Astron. Soc.* **483** (2019) L12 [1807.04335].
- [45] M. Boettcher, A. Reimer, K. Sweeney and A. Prakash, *Leptonic and Hadronic Modeling of Fermi-Detected Blazars*, *Astrophys. J.* **768** (2013) 54 [1304.0605].
- [46] ICECUBE, FERMI-LAT, MAGIC, AGILE, ASAS-SN, HAWC, H.E.S.S., INTEGRAL, KANATA, KISO, KAPTEYN, LIVERPOOL TELESCOPE, SUBARU, SWIFT NUSTAR, VERITAS, VLA/17B-403 collaboration, *Multimessenger observations of a flaring blazar coincident with high-energy neutrino IceCube-170922A*, *Science* **361** (2018) eaat1378 [1807.08816].
- [47] M. Cerruti, *Leptonic and Hadronic Radiative Processes in Supermassive-Black-Hole Jets*, *Galaxies* **8** (2020) 72 [2012.13302].
- [48] G. Ghisellini, F. Tavecchio, L. Foschini, G. Ghirlanda, L. Maraschi and A. Celotti, *General physical properties of bright fermi blazars: Properties of bright fermi blazars*, *Monthly Notices of the Royal Astronomical Society* **402** (2009) 497–518.
- [49] A. Celotti and G. Ghisellini, *The power of blazar jets*, *Mon. Not. Roy. Astron. Soc.* **385** (2008) 283 [0711.4112].
- [50] M. Gorchtein, S. Profumo and L. Ubaldi, *Probing Dark Matter with AGN Jets*, *Phys. Rev. D* **82** (2010) 083514 [1008.2230].
- [51] P. Ullio, H. Zhao and M. Kamionkowski, *A Dark matter spike at the galactic center?*, *Phys. Rev. D* **64** (2001) 043504 [astro-ph/0101481].
- [52] O.Y. Gnedin and J.R. Primack, *Dark Matter Profile in the Galactic Center*, *Phys. Rev. Lett.* **93** (2004) 061302 [astro-ph/0308385].
- [53] G.D. Alekseev et al., *The DELPHI experiment at LEP*, *Part. Nucl. Lett.* **98** (2001) 5.
- [54] L. Angel et al., *Toward a search for axionlike particles at the LNSL*, *Phys. Rev. D* **108** (2023) 055030 [2305.13384].
- [55] BABAR collaboration, *Search for a Dark Photon in e^+e^- Collisions at BaBar*, *Phys. Rev. Lett.* **113** (2014)

- 201801 [1406.2980].
- [56] J. Liu, Y. Luo and M. Song, *Investigation of the concurrent effects of ALP-photon and ALP-electron couplings in Collider and Beam Dump Searches*, *JHEP* **09** (2023) 104 [2304.05435].
- [57] G. Armando, P. Panci, J. Weiss and R. Ziegler, *Leptonic ALP portal to the dark sector*, *Phys. Rev. D* **109** (2024) 055029 [2310.05827].
- [58] Y.M. Andreev et al., *Improved exclusion limit for light dark matter from $e+e-$ annihilation in NA64*, *Phys. Rev. D* **104** (2021) L091701 [2108.04195].
- [59] NA64 collaboration, *Search for Axionlike and Scalar Particles with the NA64 Experiment*, *Phys. Rev. Lett.* **125** (2020) 081801 [2005.02710].
- [60] J.D. Bjorken, S. Eklund, W.R. Nelson, A. Abashian, C. Church, B. Lu et al., *Search for Neutral Metastable Penetrating Particles Produced in the SLAC Beam Dump*, *Phys. Rev. D* **38** (1988) 3375.
- [61] D.J. Bechis, T.W. Dombeck, R.W. Ellsworth, E.V. Sager, P.H. Steinberg, L.J. Teig et al., *Search for Axion Production in Low-energy Electron Bremsstrahlung*, *Phys. Rev. Lett.* **42** (1979) 1511.
- [62] J. Blumlein et al., *Limits on the mass of light (pseudo)scalar particles from Bethe-Heitler $e+e-$ and $\mu+\mu-$ pair production in a proton-iron beam dump experiment*, *Int. J. Mod. Phys. A* **7** (1992) 3835.
- [63] S. Andreas, O. Lebedev, S. Ramos-Sanchez and A. Ringwald, *Constraints on a very light CP-odd Higgs of the NMSSM and other axion-like particles*, *JHEP* **08** (2010) 003 [1005.3978].
- [64] Y.-S. Liu and G.A. Miller, *Validity of the Weizsäcker-Williams approximation and the analysis of beam dump experiments: Production of an axion, a dark photon, or a new axial-vector boson*, *Phys. Rev. D* **96** (2017) 016004 [1705.01633].
- [65] L. Waites, A. Thompson, A. Bungau, J.M. Conrad, B. Dutta, W.-C. Huang et al., *Axionlike particle production at beam dump experiments with distinct nuclear excitation lines*, *Phys. Rev. D* **107** (2023) 095010 [2207.13659].
- [66] P. Carena and G. Lucente, *Supernova bound on axionlike particles coupled with electrons*, *Phys. Rev. D* **104** (2021) 103007 [2107.12393].
- [67] N. Bar, K. Blum and G. D’Amico, *Is there a supernova bound on axions?*, *Phys. Rev. D* **101** (2020) 123025 [1907.05020].
- [68] E. Hardy, A. Sokolov and H. Stubbs, *Supernova bounds on new scalars from resonant and soft emission*, **2410.17347**.
- [69] M. Giannotti, I. Irastorza, J. Redondo and A. Ringwald, *Cool WISPs for stellar cooling excesses*, *JCAP* **05** (2016) 057 [1512.08108].
- [70] A. Caputo and G. Raffelt, *Astrophysical Axion Bounds: The 2024 Edition*, *PoS COSMICWISPs* (2024) 041 [2401.13728].
- [71] S. Tremaine and J.E. Gunn, *Dynamical Role of Light Neutral Leptons in Cosmology*, *Phys. Rev. Lett.* **42** (1979) 407.
- [72] K. Petraki and R.R. Volkas, *Review of asymmetric dark matter*, *Int. J. Mod. Phys. A* **28** (2013) 1330028 [1305.4939].
- [73] N. Okada, S. Okada and Q. Shafi, *Light Z' and dark matter from $U(1)_X$ gauge symmetry*, *Phys. Lett. B* **810** (2020) 135845 [2003.02667].
- [74] P. Coloma, P. Coloma, M.C. Gonzalez-Garcia, M.C. Gonzalez-Garcia, M. Maltoni, M. Maltoni et al., *Constraining new physics with Borexino Phase-II spectral data*, *JHEP* **07** (2022) 138 [2204.03011].
- [75] M. Bauer, P. Foldenauer and J. Jaeckel, *Hunting All the Hidden Photons*, *JHEP* **07** (2018) 094 [1803.05466].
- [76] D. Banerjee et al., *Dark matter search in missing energy events with NA64*, *Phys. Rev. Lett.* **123** (2019) 121801 [1906.00176].
- [77] E. Hardy and R. Lasenby, *Stellar cooling bounds on new light particles: plasma mixing effects*, *JHEP* **02** (2017) 033 [1611.05852].
- [78] D.K. Ghosh, P. Ghosh, S. Jeusun and R. Srivastava, *The N_{eff} at CMB challenges $U(1)_X$ light gauge boson scenarios*, **2404.10077**.
- [79] A. Majumdar, D.K. Papoulias and R. Srivastava, *Dark matter detectors as a novel probe for light new physics*, *Phys. Rev. D* **106** (2022) 013001 [2112.03309].
- [80] V. De Romeri, D.K. Papoulias and C.A. Ternes, *Light vector mediators at direct detection experiments*, **2402.05506**.
- [81] A.N. Khan, W. Rodejohann and X.-J. Xu, *Borexino and general neutrino interactions*, *Phys. Rev. D* **101** (2020) 055047 [1906.12102].
- [82] M. Atzori Corona, M. Cadeddu, N. Cargioli, F. Dordei, C. Giunti, Y.F. Li et al., *Probing light mediators and $(g-2)_\mu$ through detection of coherent elastic neutrino nucleus scattering at COHERENT*, *JHEP* **05** (2022) 109 [2202.11002].
- [83] M. Ibe, S. Kobayashi, Y. Nakayama and S. Shirai, *Cosmological constraint on dark photon from N_{eff}* , *JHEP* **04** (2020) 009 [1912.12152].
- [84] M. Escudero, *Neutrino decoupling beyond the Standard Model: CMB constraints on the Dark Matter mass with a fast and precise N_{eff} evaluation*, *JCAP* **02** (2019) 007 [1812.05605].
- [85] Y. Ema, F. Sala and R. Sato, *Neutrino experiments probe hadrophilic light dark matter*, *SciPost Phys.* **10** (2021) 072.
- [86] M.J. Dolan, F. Kahlhoefer, C. McCabe and K. Schmidt-Hoberg, *A taste of dark matter: Flavour constraints on pseudoscalar mediators*, *JHEP* **03** (2015) 171 [1412.5174].
- [87] S. Okada, *Z' Portal Dark Matter in the Minimal $B-L$ Model*, *Adv. High Energy Phys.* **2018** (2018) 5340935 [1803.06793].